Supplementary Information for "Finite size effects in critical fiber networks"

Sadjad Arzash,[1, 2] Jordan L. Shivers,[1, 2] and Fred C. MacKintosh[1, 2, 3]

[1] *Department of Chemical & Biomolecular Engineering, Rice University, Houston, TX 77005*
[2] *Center for Theoretical Biological Physics, Rice University, Houston, TX 77030*
[3] *Departments of Chemistry and Physics & Astronomy, Rice University, Houston, TX 77005*

Network models
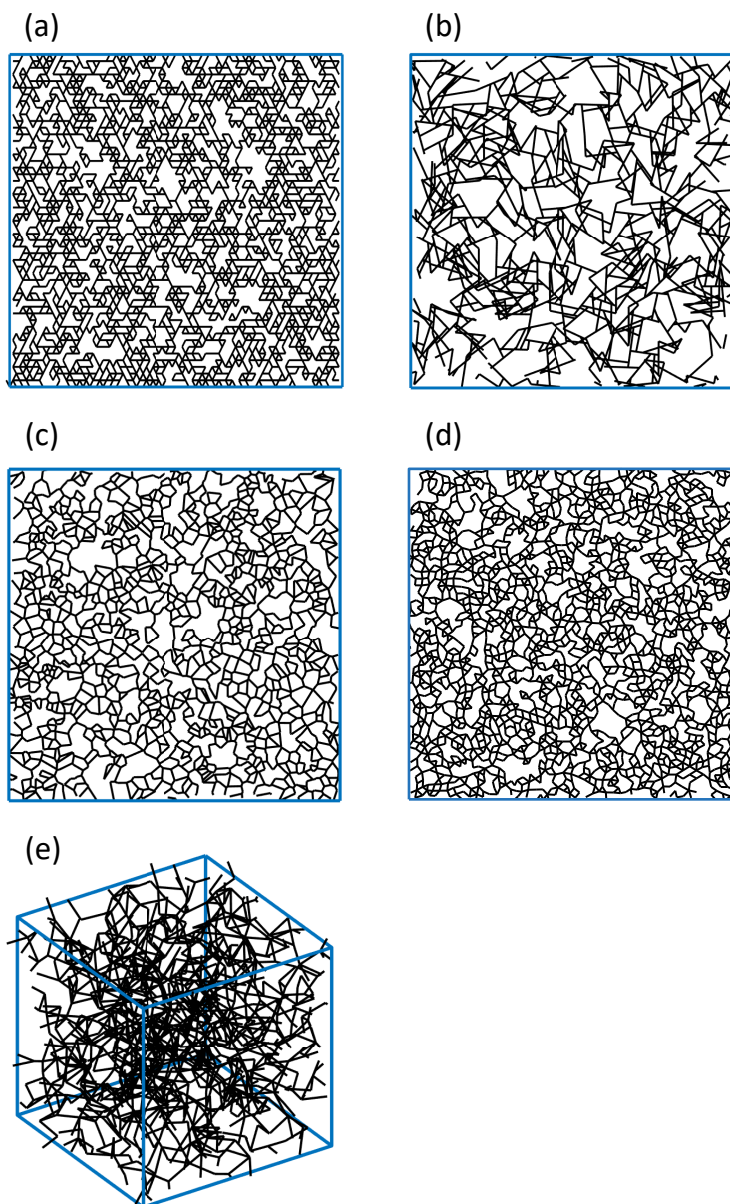
FIG. S.1. Snapshots of various network models. (a) Randomly diluted triangular network with $z = 3.3$. (b) Randomly diluted Mikado model with $z = 3.3$. (c) Randomly diluted 2D Voronoi network with $z = 2.6$. (d) Randomly diluted 2D jammed-packing-derived network with $z = 3.3$. (e) Randomly diluted 3D jammed-packing-derived network with $z = 3.3$.
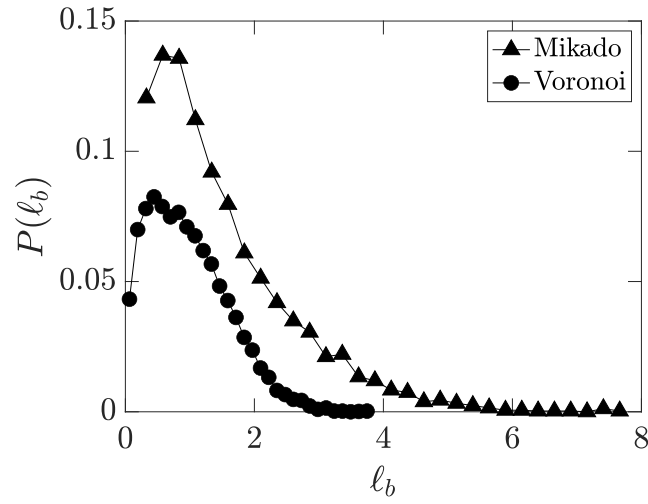
FIG. S.2. The bond length distribution of Mikado and Voronoi models. These exponential-like decay of bond length has been identified in real collagen networks.
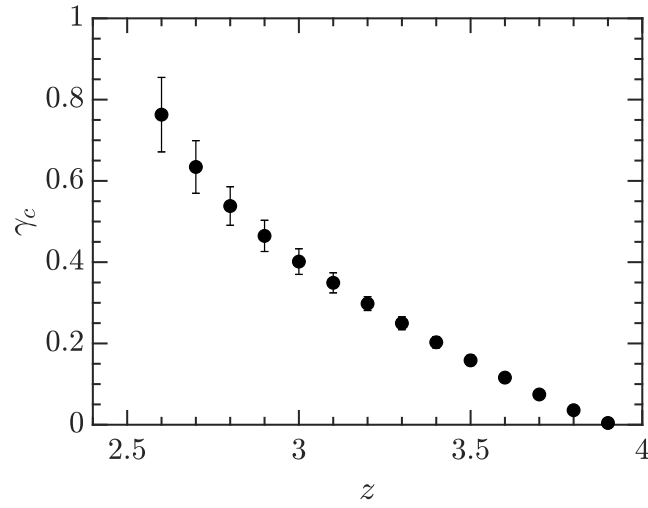
FIG. S.3. The critical strain versus connectivity for a randomly diluted triangular network with size $W = 80$. Near the isostatic point z_c, the relation appears to be linear. Note that $z_c < 4.0$ is due to the finite size effects.

Scaling of the moments of force distributions
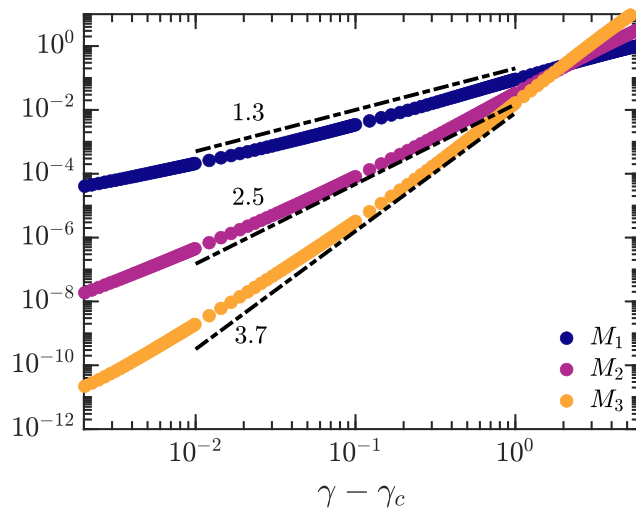
FIG. S.4. The scaling behavior of first three moments of force distribution versus excess strain to the critical point for a triangular network with $z = 3.3$.

Nonaffine displacement fluctuations

In order to find the correlation length exponent ν, we compute the nonaffine fluctuations in athermal fiber networks. The differential non-affinity parameter $\delta\Gamma$ defined in Eq. 7 measures the nonaffine node displacements after applying a small shear strain from a previous state.
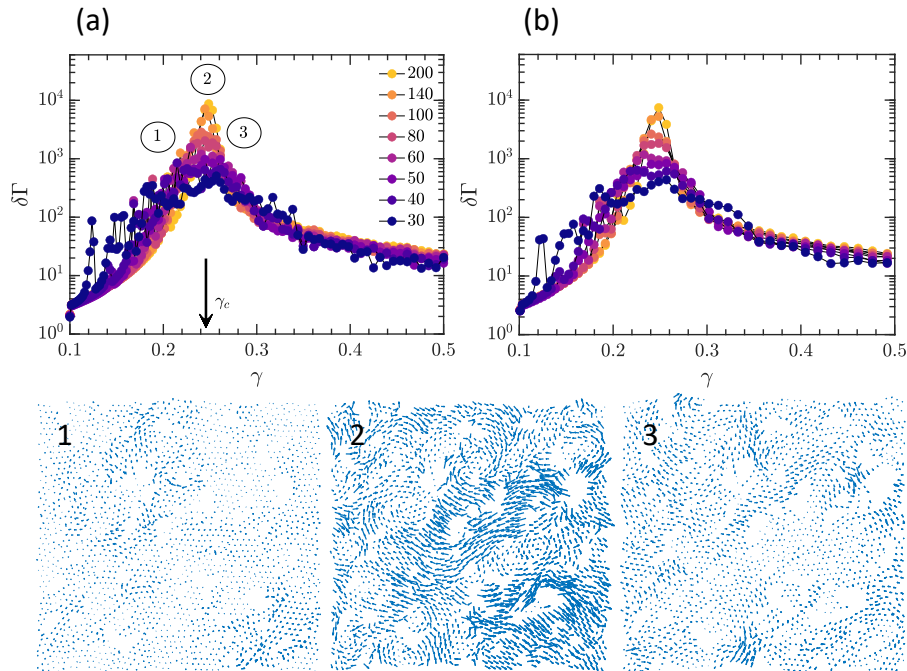
FIG. S.5. (a) The unscaled differential non-affinity parameter defined in Eq. 7 in the main text for diluted triangular networks with $z = 3.3$ and sizes as shown in the legend. The nonaffine displacement vectors of a single sample of size $W = 50$ are shown for a strain value less than (1) at (2) and greater than (3) the critical strain γ_c. (b) Coarse-grained $\delta\Gamma$, using local averaging of every two adjacent data points in (a).

Figure S.5 a shows the differential non-affinity for diluted triangular network with $z = 3.3$ for different system sizes. The nonaffine vectors of network's nodes for a single sample of size $W = 50$ are shown at (1): $\gamma < \gamma_c$ (2): $\gamma = \gamma_c$ (3): $\gamma > \gamma_c$. As we can see from the displacement field, large nonaffine node displacements are evident at the

critical strain, which corresponds to the peak in differential non-affinity parameter. In order to reduce the noise in $\delta\Gamma$ for finite-size scaling, we use the local averaging method; every two adjacent values of Fig. S.5 a are averaged and the result is shown in Fig. S.5 b. The finite-size collapse shown in Fig. 4 in the main text is indeed the collapse of coarse-grained data in Fig. S.5 b.

Finite size analysis of the participation ratio ψ

The distribution of participation ratio at the critical strain ψ_c is shown in Fig. S.6 for diluted triangular networks at various sizes. The distribution appears to be bimodal: the large peak is related to the branch-like force chains in the network, similar to the structure shown in Fig. 3 a, and the small peak at low participation ratio, which is due to the finite-size effects. Although the location of large peak depends on the network connectivity z, the small peak is the result of a small number of realizations that shows a tensional path at the critical strain connecting upper and lower sides of the periodic box. This tension line yields a plateau behavior in stiffness of the network (see Fig. S.7 a). As system size increases, the number of samples with this small tensional structure decreases and disappears completely in the thermodynamic limit. This tensional pattern is shown for a single sample in Fig. S.7 b.
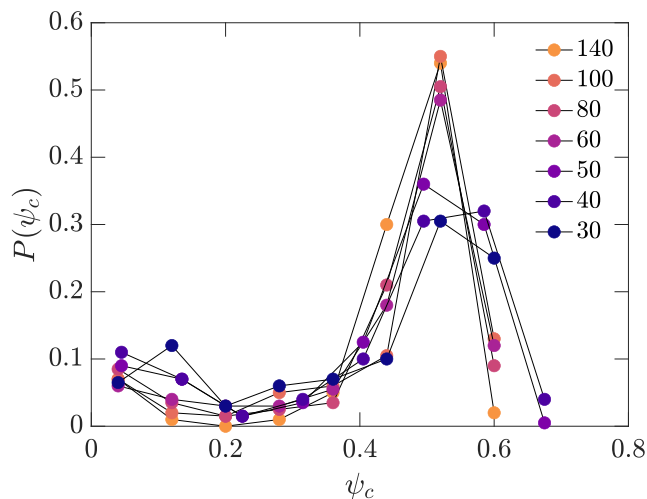
FIG. S.6. The distributions of critical participation ratio ψ_c for different sizes of a triangular network with $z = 3.3$.
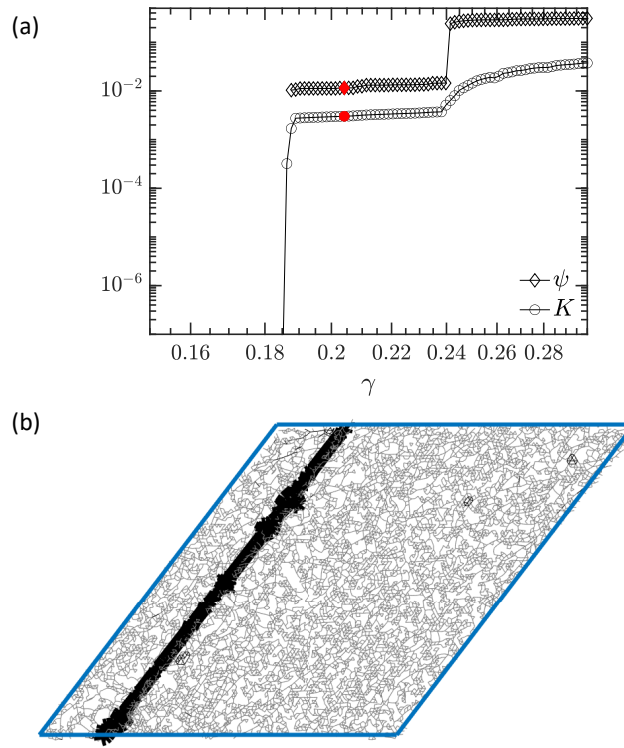
FIG. S.7. (a) The participation ratio ψ and stiffness K for a single random realizations with a plateau effect for diluted triangular model with $z = 3.3$ and $W = 100$. (b) The tensional line responsible for the plateau effect near the critical strain in (a) is shown by plotting bonds with a thickness proportional to their tensions at the highlighted strain point in (a).
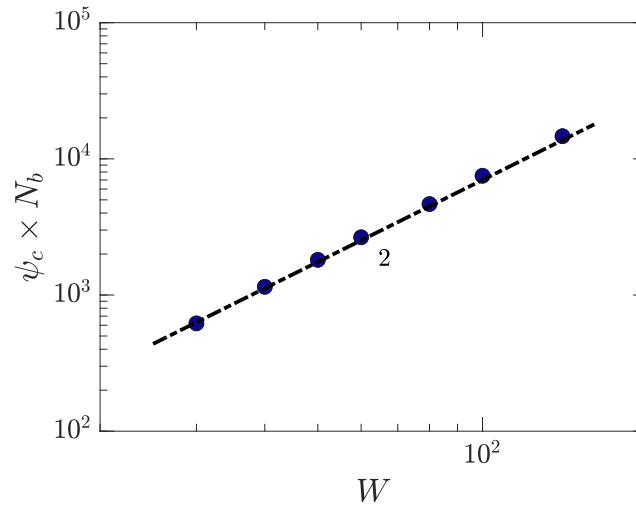
FIG. S.8. The critical participation ratio times the number of bonds, which is a measure of mass of the tensional structure at the critical point, versus network size for a triangular model with $z = 3.3$.

Finite size effects on the scaling exponent f
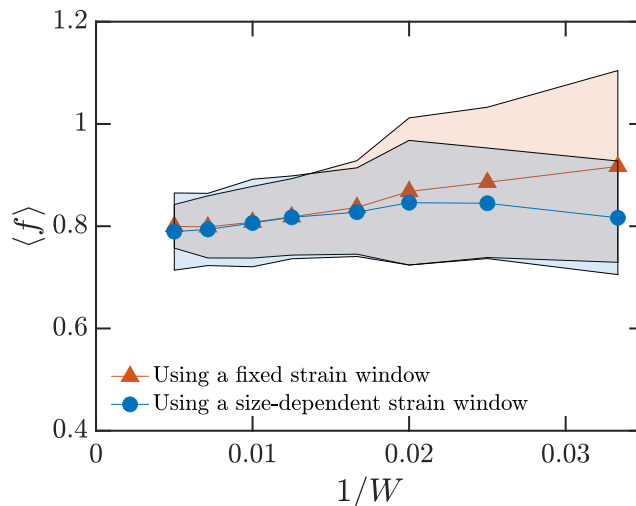
FIG. S.9. Comparing two methods of finding f for different sizes of a triangular network with $z = 3.3$. The shadow area is showing the standard deviations. The red triangles correspond to the exponents that are obtained in a fixed strain window for all sizes, here the strain window is $\Delta\gamma = 0.055 - 1.0$. The blue circles correspond to the exponents we obtained in a size-dependent strain window in which $1.0 < |\Delta\gamma| \times W^{1/\nu} < 30$ for all sizes.

f exponent for a 3D network

We obtain $f = 0.84 \pm 0.13$ for 3D jammed-packing-derived model with $z = 3.3$. The data are collected for only one system size $W = 20$, averaging over 40 random samples. Assuming the hyperscaling relation $f = d\nu - 2$ holds in 3D, we used $\nu = (f + 2)/3 \cong 0.95$ for the following scaling plot. This network has $\gamma_c = 0.57 \pm 0.03$ and $K_c = 0.006 \pm 0.004$. Future studies will be needed in 3D for a detailed finite-size scaling analysis similar to Fig. 9 in the main text as well as testing the hyperscaling relation $f = d\nu - 2$.
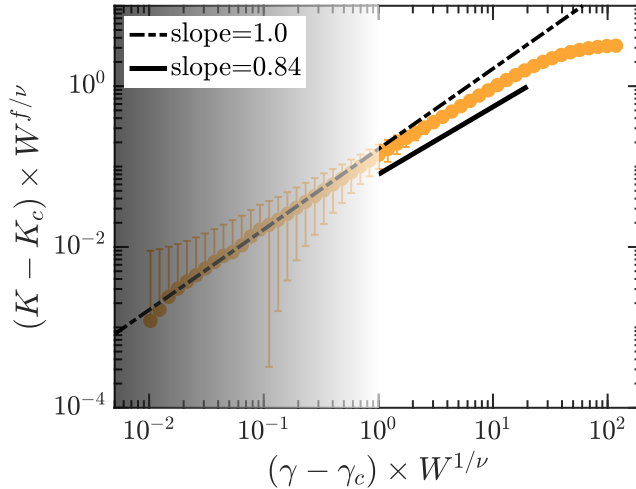
FIG. S.10. Finite-size effects for a 3D packing-derived network with $z = 3.3$ and $W = 20$. In the critical region, we find a non-mean-field exponent $f = 0.84$. The finite-size dominated region is shaded.

The effect of K_c on the exponent f

The scaling exponent f, which is obtained in the critical regime, is robust to errors in the value of discontinuity K_c. Figure S.11 shows that choosing different values for K_c in a triangular network has negligible effect on f. Although the jammed-packing-derived model exhibits a slope of 1.0 in the finite-size dominated region, the triangular model

behaves differently (see Fig. 9). This is due to the fact that in contrast to packing-derived networks, triangular networks are likely to be rigidified by a single straight path of bonds connecting upper and lower boundaries of the simulation box in the small strain regime. Therefore, the K_c values for a triangular network that are observed for small strains are results of these strand-like tensions. As we increase the strain, more bonds become involved, thus the slope in the finite-size dominated region gets closer to 1.0, similar to packing-derived networks. This is clearly observed by choosing different K_c values for finite-size scaling analysis of triangular networks (see Fig. S.11).
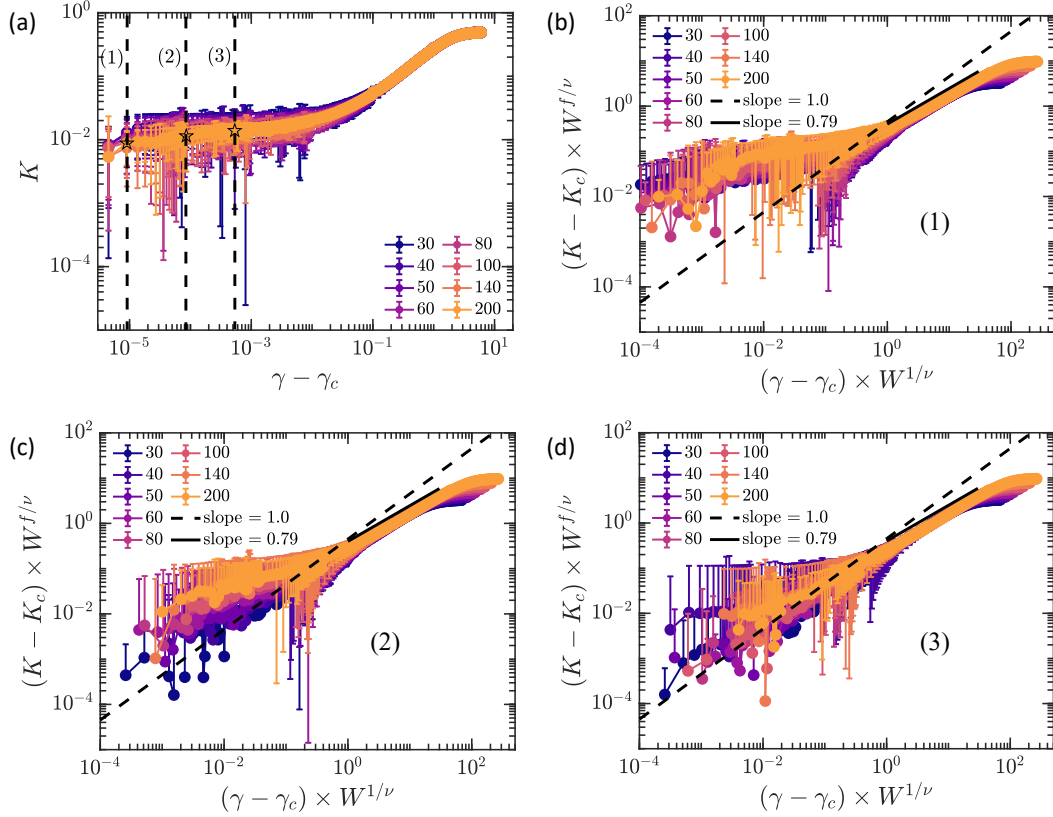
FIG. S.11. (a) Differential shear modulus versus $\gamma - \gamma_c$ for triangular networks with $z = 3.3$. Plots (b)-(d) show the scaling analysis of the data in (a) using K_c values corresponding to $\gamma - \gamma_c$ at vertical lines (1)-(3) in plot (a).

By using the modulus discontinuity in the thermodynamic limit K_c^∞, we repeat the analysis performed in Fig. 9 a in the main text. As can be observed in Fig. S.12, we find the same non-mean-field scaling exponent f.
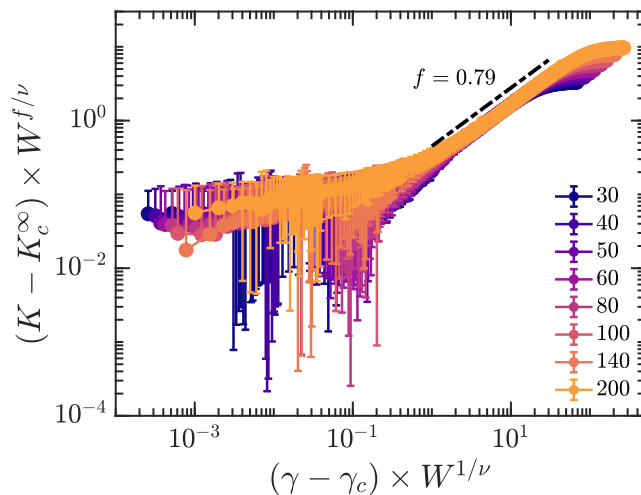
FIG. S.12. Finite-size scaling of the data in Fig. 9 a in the main text, using K_c in the thermodynamic limit.

Fiber networks with bending interactions

Using central force networks, we are only able to investigate the positive side of the transition, i.e., $\gamma - \gamma_c \to 0^+$. In order to understand the system's behavior below the critical point, we stabilize the networks by introducing weak bending interactions between bonds. Therefore, the elastic energy for the network has both stretching E_s and bending E_b contributions

$$E = E_s + E_b = \frac{\mu}{2} \sum_{ij} \frac{(\ell_{ij} - \ell_{ij,0})^2}{\ell_{ij,0}} + \frac{\kappa}{2} \sum_{ij} \frac{(\theta_{ijk} - \theta_{ijk,0})^2}{\ell_{ijk,0}}, \tag{S.1}$$

in which the stretching part E_s is the same as in Eq. 1 in the main text, κ is the bending stiffness of individual fibers, $\theta_{ijk,0}$ is the angle between bonds ij and jk in the undeformed state, θ_{ijk} is the angle between those bonds after deformation, and $\ell_{ijk,0} = \frac{1}{2}(\ell_{ij,0} + \ell_{jk,0})$. Note that the bending energy is defined for consecutive bonds along each fiber on the triangular lattice. In simulations, we set $\mu = 1.0$ and vary the dimensionless bending stiffness $\tilde{\kappa} = \kappa/\mu\ell_0^2$, where ℓ_0 is the typical bond length ($\ell_0 = 1$ in lattice models).

The simulation procedure for networks with bending interactions is basically the same as discussed in the main text for central force networks. The differential shear modulus K versus shear strain is shown in Fig. S.13 a for various dimensionless bending rigidity $\tilde{\kappa}$.
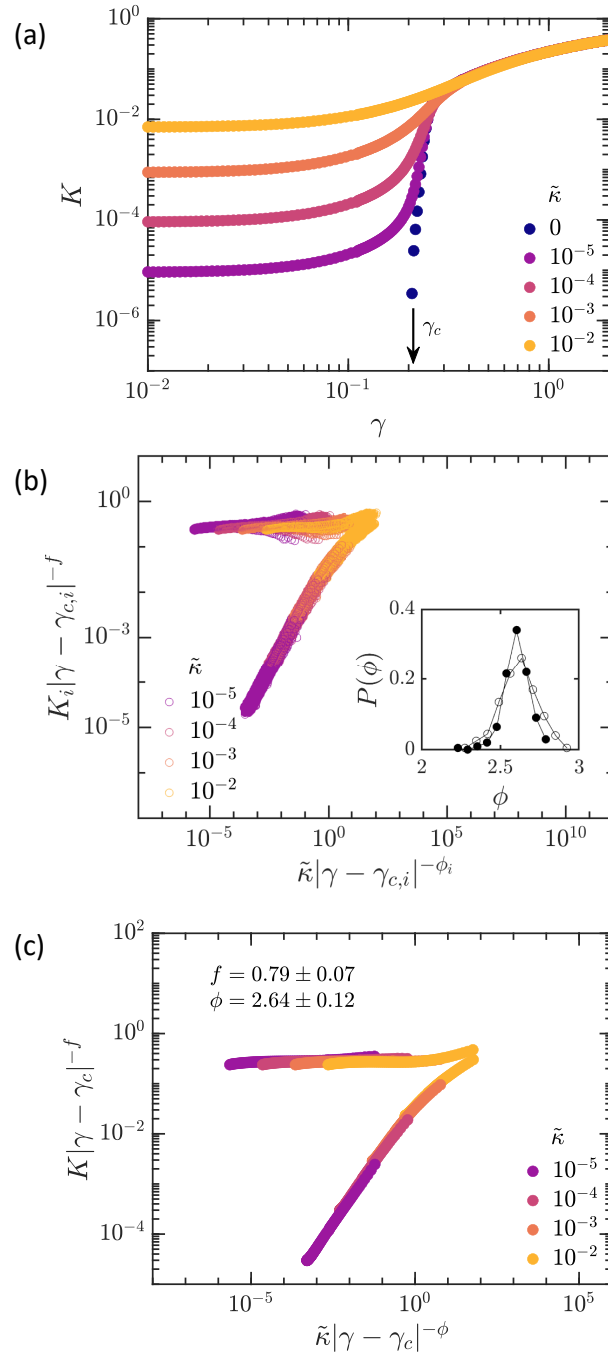
FIG. S.13. (a) The differential shear modulus versus strain for triangular networks with $W = 100, z = 3.3$ and varying the dimensionless bending rigidity $\tilde{\kappa}$. (b) The Widom-like collapse of individual samples in (a) according to Eq. 7 in the main text using the exponent f that is already obtained for central force networks. Note that the finite-size-dominated data in which $|\Delta\gamma| \times W^{1/\nu} < 1.0$ are removed from this plot. Inset: showing the distribution of ϕ, which are collected in $\gamma < \gamma_c$ regime of Eq. 7 in the main text. The ϕ values here are obtained using data with $\tilde{\kappa} = 10^{-5}$. The solid symbols are corresponding to ϕ values obtained using the ensemble average f, the empty symbols, on the other hand, are the distribution of ϕ exponents that collected using sample-specific f. (c) The Widom-like collapse similar to (b), but for the ensemble average of data. We note that the finite-size-dominated data in which $|\Delta\gamma| \times W^{1/\nu} < 1.0$ are removed from this plot.